Communications on Applied Nonlinear Analysis
ISSN: 1074-133X
Vol 32 No. 9s (2025)

Study of Convective Magnetohydrodynamic Flow of Casson Fluids through a Porous Medium Incorporating the Darcy-Forchheimer Model and Influenced by Prescribed Heat Sources

Avinash B. Raut[1,2], Pradeep G Janthe[1], Jagadish V. Tawade[1,*]

[1]Department of Mathematics, Vishwakarma University, Pune, India

[2]Department of Engineering Sciences & Humanities, Vishwakarma Institute of Technology, Pune, India

avinash.raut@vit.edu,

pradeepjanthe@gmail.com,

jagadish.tawade@vupune.ac.in

Article History:

Received: 12-01-2025

Revised: 15-02-2025

Accepted: 01-03-2025

Abstract:

This study investigates the heat and mass transfer properties of a 2D electrically conducting incompressible Casson fluid flowing through a porous medium over a stretching sheet. The analysis considers the effects of a magnetic field, heat generation/absorption, and chemical reactions. The Casson fluid model is employed to describe the non-Newtonian behaviour of the fluid, which is relevant in biomechanics and polymer industries due to its yield stress. A numerical simulation is performed to estimate the flow of a Casson nanofluid over a stretching surface. The governing boundary layer equations are transformed into ordinary differential equations using a stream function formulation and solved numerically using the BVP4C method.

The results show that the non-dimensional parameters significantly affect the energy, concentration, and velocity profiles. The yield stress of the Casson fluid is found to impact the flow resistance, velocity, and temperature profiles, differing from those of Newtonian fluids. Specifically, higher yield stress leads to lower velocity fields and altered thermal profiles.

Keywords: Magnetohydrodynamic, Casson Nanofluid; Darcy–Forchheimer model, Heat Source/Sink, Porous medium, Unsteady parameter, Prescribed heat source.

Introduction:

Significant attention has been given to studying the flow dynamics and heat transfer characteristics of a stretching sheet within the boundary layer. The analysis of flow over a sheet undergoing stretching is crucial for various engineering applications, particularly in fields like metallurgy. Fluid dynamics has become an essential area of scientific research in modern times, fueling innovations across industries such as aerospace, automotive, civil engineering, environmental science, biomedical engineering, oil and gas, chemical engineering, and sports. These interdisciplinary applications underscore the profound influence of fluid dynamics research on contemporary technology and society.

Nonuniform heating has proven effective in controlling transport phenomena in complex systems. One approach involves using nonuniform heating based on a half-sinusoidal pattern, with or without a

temperature offset. This technique is widely applicable in fields like heat exchangers, mixing industries, crystal growth, material processing, pharmaceuticals, medical devices, and electronic cooling. The complexity of convective dynamics under nonuniform heating is heightened by factors such as geometry, orientation, boundary conditions, and multiphysics interactions. However, there is limited literature addressing these concepts.

Sakiadis, Byron C. [1] investigated boundary-layer behavior on continuous solid surfaces, while Crane [2] studied the heat transfer and flow dynamics of electrically conductive, viscous fluids over a stretched fluid layer. Farooq et al. [3] explored the impact of non-similar modeling on the Darcy-Forchheimer-Brinkman model for forced convection of Casson nanofluid in non-Darcy porous media. Shoaib et al. [4-5] examined MHD Casson nanofluid flow in a Darcy-Forchheimer porous medium with heat source and Arrhenius activation energy, applying neural networks, and also studied the effects of thermal energy on MHD Casson fluid through a Forchheimer porous medium with an inclined non-linear surface using a soft computing approach.

Farooq et al. [6] investigated the modeling and non-similar analysis of the Darcy-Forchheimer-Brinkman model for Casson fluid flow in a porous medium. Seth et al. [7] explored double-diffusive MHD Casson fluid flow in a non-Darcy porous medium with effects of Newtonian heating and thermo-diffusion. Durairaj et al. [8] examined heat generating/absorbing and chemically reacting Casson fluid flow over a vertical cone and flat plate, saturated in a non-Darcy porous medium. Jat et al. [9] analyzed the significance of Darcy–Forchheimer Casson fluid flow past a non-permeable curved stretching sheet, considering heat and mass transfer impacts. Waheed et al. [10] studied unsteady magnetohydrodynamic squeezing Darcy-Forchheimer flow of Fe3O4 Casson nanofluid, examining the effects of heat source/sink and thermal radiation.

Sharma et al. [11] investigated the dynamics of MHD Casson fluid in a non-Darcy porous medium, with the impact of thermal radiation, Dufour-Soret effects, and chemical reactions. Ragupathi et al. [12] applied Arrhenius kinetics to MHD radiative Von Kármán Casson nanofluid flow in a Darcy-Forchheimer porous medium with an adjustable heat source. Li, Shuguang, et al. [13] examined the effects of activation energy and chemical reaction on unsteady MHD dissipative Darcy–Forchheimer squeezed flow of Casson fluid in a horizontal channel. Faisal et al. [14] conducted numerical assessments of prescribed heat sources on unsteady 3D flow of Williamson nanoliquid through porous media. Tufail et al. [15] explored chemically reacting mixed convective Casson fluid flow in the presence of MHD and a porous medium through group theoretical analysis.

Mohamed, R. A., et al. [16] studied MHD Casson nanofluid flow over a stretching surface embedded in a porous medium, considering thermal radiation and slip conditions. Ramesh et al. [17] examined the Darcy-Forchheimer flow of Casson nanofluid with heat source/sink in a three-dimensional context. Abbas et al. [18] analyzed the influence of Darcy-Forchheimer relation on MHD dissipative third-grade fluid flow and heat transfer in porous media with Joule heating effects using a numerical approach. Kala, Bhim Sen et al. [19] conducted a numerical investigation of the effects of Darcy and Forchheimer parameters on Magnetohydrodynamic Casson fluid flow through non-Darcy porous media. Eid, Mohamed R. [20] examined the thermal characteristics of 3D nanofluid flow over a convectively heated Riga surface in a Darcy-Forchheimer porous material, considering linear thermal radiation and optimal analysis.

Shampine et al. [21] presented methods for solving boundary value problems for ordinary differential equations in MATLAB with the bvp4c solver. Devi and Sood [22] investigated convective MHD flow of Casson fluid through a porous medium using the Darcy-Forchheimer model, under the influence of prescribed heat sources. Mustafa et al. [23] studied unsteady boundary layer flow of Casson fluid due to an impulsively started moving flat plate. Eldabe et al. [24] explored heat transfer in MHD non-Newtonian Casson fluid flow between two rotating cylinders. Ishak et al. [25] studied mixed convection at the stagnation point flow toward a vertical, continuously stretching sheet. Bejawada et al. [26] examined the radiation effect on MHD Casson fluid flow over an inclined non-linear surface with chemical reactions in a Forchheimer porous medium. Thakur et al. [27] analyzed the effect of prescribed heat sources on convective unsteady MHD flow of Williamson nanofluid through porous media. Majeed et al. [28] investigated unsteady ferromagnetic liquid flow and heat transfer analysis over a stretching sheet, considering the effect of dipole and prescribed heat flux.

This study investigates the convective heat transfer dynamics of Casson fluid flow through porous media under the influence of a nonuniform horizontal magnetic field. By examining the complex interplay between mixed convection, Lorentz force, porous media, and spatially variable heating, this research provides fundamental insights into thermo-fluid dynamics. Key contributions include identifying optimal control parameters for enhanced thermal performance and elucidating the flow dynamics. These findings contribute significantly to thermo-fluid research, offering valuable insights for designing improved heat transfer systems with applications in various engineering fields.

Mathematical Formulation:

The present study considers an unsteady Casson nanofluid flow in a porous space, where the fluid flows past a bidirectional stretched surface in the stagnation region

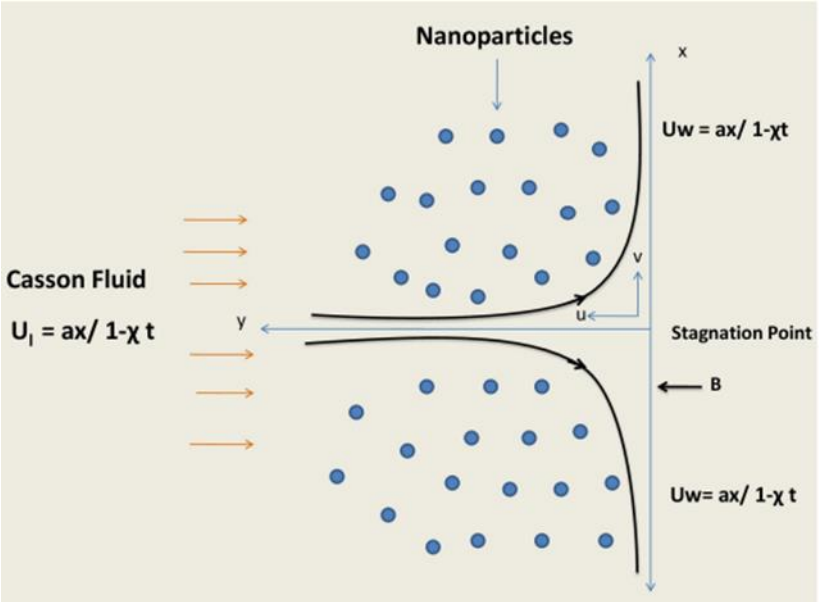

Figure 1. Physical configuration of the study.

The heat transfer analysis is performed under both PST and PHF conditions, with the fluid flowing parallel to the y-axis.

An unsteady magnetic field is enforced along the surface. The equation of state for the Casson Fluid in an isotropic flow is given by Mustafa [23] as:

$$\tau_{ij} = \begin{cases} \left(2\mu_B + \frac{\tau_y}{\sqrt{2\Pi}}\right) e_{ij}, & for\ \pi \geq \pi_c \\ \left(2\mu_B + \frac{\tau_y}{\sqrt{2\Pi}}\right) e_{ij}, & for\ \pi \leq \pi_c \end{cases}$$

The mathematical formulation of the problem is based on the following governing equations, which represent the conservation of mass, momentum, energy, and concentration:

$$\frac{\partial u}{\partial x} + \frac{\partial v}{\partial y} = 0 \qquad (1)$$

$$\frac{\partial u}{\partial t} + u\frac{\partial u}{\partial x} + v\frac{\partial u}{\partial y} = \frac{dU_1}{dx}U_1 + \frac{dU_1}{dt} + \left(1 + \frac{1}{\beta_1}\right)\nu\frac{\partial^2 u}{\partial y^2}$$

$$+ F\left({U_1}^2 - u^2\right) + \frac{\sigma {B_0}^2}{\rho}(U_1 - u) + \frac{\nu}{k^*}(U_1 - u) + (\mathrm{T} - \mathrm{T}_\infty)g\beta_T{}^* + (\mathrm{C} - \mathrm{C}_\infty)g\beta_C{}^* \qquad (2)$$

$$\frac{\partial T}{\partial t} + u\frac{\partial T}{\partial x} + v\frac{\partial T}{\partial y} = \alpha\frac{\partial^2 T}{\partial y^2} + \frac{\rho_P C_P}{(\rho C)}\left[D_B\left(\frac{\partial C}{\partial y}\frac{\partial T}{\partial y}\right) + \frac{D_T}{T_\infty}\left(\frac{\partial T}{\partial y}\right)^2\right] + \frac{\sigma B_0^2}{\rho C_P}\mathrm{u}^2 + \frac{q'''}{\rho C_P} \qquad (3)$$

$$\frac{\partial C}{\partial t} + u\frac{\partial C}{\partial x} + v\frac{\partial C}{\partial y} = D_B\left(\frac{\partial^2 C}{\partial y^2}\right) + \frac{D_T}{T_\infty}\left(\frac{\partial^2 T}{\partial y^2}\right) \qquad (4)$$

The corresponding boundary conditions are as follows:

$$u = U_w = \frac{ax}{1 - xt}\ ;\quad v = 0\ ;\quad C = C_w = C_\infty + \frac{Ax}{1 - xt} \quad \text{at } y = 0$$

$$T = T_w(x);$$

$$u = U_1 = \frac{bx}{1 - xt}$$

Where,

$$T = T_w = T_\infty + \frac{Sx}{1 - xt} \qquad \text{(PST)}$$

$$-k\frac{\partial T}{\partial y} = q_w = T_\infty + \frac{Dx}{1 - xt} \quad \text{(PHF)} \qquad (5)$$

$$T \to T_\infty;\ C \to C_\infty \qquad \text{as } y \to \infty$$

Here, $\upsilon = \frac{\mu}{\rho}$, $B = \frac{B_0}{\sqrt{1-xt}}$, $k^* = k_0(1 - \chi t), xt < 1, k_0$ gives initial permeability. Ambient fluid concentration and temperature are C_∞ and T_∞ correspondingly. $F = \frac{C_b}{x\sqrt{k^*}}$ is the porous medium's non-

uniform inertia coefficient. $\beta_C{}^*$ and $\beta_T{}^*$ indicate the concentration and thermal expansion coefficients, respectively.

Similarity transformations are employed to transform the nonlinear PDEs into ODEs, with the corresponding boundary conditions being

$$\psi = \sqrt{\frac{a\nu}{1-\chi t}}\, x f(\eta),\ \ \eta = \sqrt{\frac{a}{\nu(1-\chi t)}},$$

$$\theta(\eta) = \frac{\mathrm{T}-\mathrm{T}_\infty}{\mathrm{T}_\mathrm{w}-\mathrm{T}_\infty}, m(\eta) = \frac{\mathrm{T}-\mathrm{T}_\infty}{\mathrm{T}_\mathrm{w}-\mathrm{T}_\infty}, \phi(\eta) = \frac{\mathrm{C}-\mathrm{C}_\infty}{\mathrm{C}_\mathrm{w}-\mathrm{C}_\infty} \tag{6}$$

By adding the stream function ψ so that $u = \partial\psi/\partial y$ as well as $v = -\partial\psi/\partial x$, f , φ represent functions of η as[27],

The transformed ODE's are as follows after applying the similarity transformations:

$$ff'' + (\varepsilon - f')(\lambda + M) + f'''\left(1 + \frac{1}{\beta_1}\right) - f'^2 + \varepsilon^2 + F_r\left(\varepsilon^2 - f'^2\right) - \zeta\left(\frac{\eta}{2}f'' + f' - \varepsilon\right) + G(N\phi + \theta) = 0 \tag{7}$$

$$\theta'' - P_r\left[\zeta\left(\frac{\eta}{2}\theta' + \theta\right) + f'\theta - f\theta'\right] + \frac{N_C\phi'\theta'}{Le} + \frac{N_C\,\theta'^2}{Le\,N_{bt}} + PrJf'^2 + (A^*f' + B^*\theta) = 0 \tag{8}$$

$$m'' - P_r\left[\zeta\left(\frac{\eta}{2}m' + m\right) + f'm - fm'\right] + \frac{N_C\phi'm'}{Le} + \frac{N_C\,m'^2}{Le\,N_{bt}} + PrJf'^2 + (A^*f' + B^*m) = 0 \tag{9}$$

$$\phi'' + \frac{1}{N_{bt}}\theta'' - Sc\left[\zeta\left(\frac{\eta}{2} + f'\phi - f\phi'\right)\right] = 0 \tag{10}$$

The boundary conditions are:

PST Case:

$$f(\eta) = 0,\ f'(\eta) = 1,\ \theta(\eta) = 1,\ \phi(\eta) = 1;\ \text{at}\ \eta = 0$$
$$f'(\eta) \to \varepsilon,\ \theta(\eta) \to 0, \phi(\eta) \to 0\ \text{at}\ \eta = \infty \tag{11}$$

PHF Case:

$$f(\eta) = 0,\ f'(\eta) = 1,\ m'(\eta) = -1,\ \phi(\eta) = 1;\ \text{at}\ \eta = 0$$
$$f'(\eta) \to \varepsilon,\ m(\eta) \to 0, \phi(\eta) \to 0\ \text{at}\ \eta = \infty \tag{12}$$

The dimensionless parameters are:

Where

$$Fr = \frac{C_b}{\sqrt{k^*}}, M = \frac{\sigma B_0^2}{\rho a}, G = \frac{Gr_x}{Re_x{}^2}, \lambda = \frac{\upsilon}{k_0 C}, \xi = \frac{\chi}{C}, \varepsilon = \frac{b}{a}, J = M.Ec$$

$$N=\frac{\beta_c(C_w-C_\infty)}{\beta_T(T_w-T_\infty)}, Nc=\frac{\beta_c^*(C_w-C_\infty)}{\beta_T^*(T_w-T_\infty)}, N_{bt}=\frac{T_\infty D_B(C_w-C_\infty)}{D_T(T_w-T_\infty)}, Sc=\frac{\nu}{D_B}, \beta_1=\frac{\mu_\beta\sqrt{2\pi}}{\tau_y},\ \lambda=\frac{\nu}{k_0 a}$$

Here Fr indicates Forchheimer number, M is magnetic field parameter, λ defines permeability parameter, G defines thermal convection parameter, ζ indicates unsteadiness, N characterizes buoyancy ratio parameter, Nbt expresses diffusivity parameter, Sc defines Schmidt number, ε manifests velocity ratio parameter, Gr_x defines thermal buoyancy parameter and β_1 shows casson fluid parameter.

The following expressions define the skin friction coefficient, local Nusselt number, and Sherwood number

$$C_{fx}=\frac{{\tau_w}^*}{\rho {U_w}^2(x)}, N_{ux}=\frac{x{q_w}^*}{k(\mathrm{T_w}-\mathrm{T_\infty})}, S_{hx}=\frac{x{q_m}^*}{D_B(\mathrm{C_w}-\mathrm{C_\infty})}$$

Here Casson nanofluid's shear stress at the wall's surface is calculated ${\tau_w}^*$,while ${q_m}^*$ as well as ${q_w}^*$ provide the mass and heat fluxes from the wall, respectively. These are the terms listed as Applying similarity transformations along with dominated boundary conditions leads to the description of above mentioned parameters in their non-dimensional forms:

$$C_{fx}(Re)^{\frac{1}{2}}=\left(1+\frac{1}{\beta_1}f''(0)\right)$$

$$N_{ux}(Re)^{-\frac{1}{2}}=\begin{cases}\left(-\theta'(\eta)\right)\ at\ \eta=0, PST\ case\\ \left(\frac{1}{m(\eta)}\right)at\ \eta=0, PHF\ case\end{cases}$$

$$S_{hx}(Re)^{-\frac{1}{2}}=\left(-\phi'(\eta)\right)\ at\ \eta=0$$

Reynolds number in this case is $Re=\frac{U_w(x)}{\upsilon(1-\gamma t)}$.

Mathematical Formulation:

This research has discussed a bvp4c explanatory implementation for the study under consideration. By applying similarity transformations, we converted the PDE system into a set of ODEs, and subsequently utilized MATLAB's bvp4c solver to obtain the solution. The process demonstration was provided by Shampine [21].

Step-1:

For Prescribed Surface Temperature Case:

$$f=y_1, f'=y_2, f''=y_3, \theta=y_4, \theta'=y_5, \phi=y_6, \phi'=y_7$$

Prescribed Heat Flux Case

$$f=y_1, f'=y_2, f''=y_3, \theta=y_4, \theta'=y_5, \phi=y_6, \phi'=y_7$$

Step-2:

$$f''' = \frac{-y_1 y_3 + {y_2}^2 - \varepsilon^2 - (\varepsilon - y_2)(\lambda + M) - Fr(\varepsilon^2 - {y_2}^2) + \zeta\left(\frac{\eta}{2} y_3 + y_2 - \varepsilon\right) - G(y_4 + N y_6)}{1 + \frac{1}{\beta_1}}$$

For PST Case:

$$\theta'' = Pr\left[\zeta\left(\frac{\eta}{2} y_5 + y_4\right) - y_1 y_5 + y_2 y_4\right] - \frac{Nc}{Le} y_7 y_5 - \frac{Nc}{Le\, Nbt} {y_5}^2$$

For PHF Case:

$$m'' = Pr\left[\zeta\left(\frac{\eta}{2} y_5 + y_4\right) - y_1 y_5 + y_2 y_4\right] - \frac{Nc}{Le} y_7 y_5 - \frac{Nc}{Le\, Nbt} {y_5}^2$$

$$\phi'' = Sc\left[\left(\zeta\left(\frac{\eta}{2} y_7 + y_6\right)\right) + y_2 y_6 - y_1 y_7\right] - \frac{1}{Nbt}$$

Step-3:

The boundary conditions change as a consequence of new variables:

$y_1' = 0, y_2' = 1, y_4' = 1, y_6' = 1, y_2'' = \varepsilon, y_4'' = 0, y_6'' = 0$ (PST Case)

$y_1' = 0, y_2' = 1, y_5' = -1, y_6' = 1, y_2'' = \varepsilon, y_4'' = 0, y_6'' = 0$ (PHF Case)

Step-4:

In this case, w' characterizes position at $\eta = 0$ whereas w^u characterizes position as $\eta \to \infty$.

MATLAB's bvp4c solver is used to resolve the system of 1st-order equations using boundary conditions. To maintain accuracy, initial assumptions, boundary layer edge position, and step size are changed as necessary.

In our study, we have investigated heat transfer and the impacts of many increase in physical parameters including $\varepsilon, Le, Pr, Sc, Nc, N_{bt}, \beta_1, \lambda, Fr, G$, N and ζ on temperature $\theta(\eta)$, velocity $f'(\eta)$, as well as nanoparticle concentration profiles $\varphi(\eta)$ and the findings were shown by figures.

Code verification:

With a few previously published studies, we have compared our results to make sure our assumptions are reasonable and our code is reliable. Comparative study of f''(0) values for different ε values givenin Table -1 in such a way that ζ = G = N = β 1 = 0 = Fr = λ = M. The obtained results are in good accord with the work of Thakur& Sood [27], Hayat et al. [28], and Devi and Sood [22].

Table 1: Comparative $f''(0)$ values for distinct ε values

S	Thakur & Sood [27]	Hayat et al. [28]	Devi and Sood [22]	Present study
0.1	-0.9694	-0.9694	-0.9694	-0.9694
0.2	-0.9181	-0.9181	-0.9181	-0.9181

0.5	-0.6673	-0.6673	-0.6673	-0.6673
2	2.0176	2.0176	2.0187	2.0187

Findings:

We considered the parameter values in the numerical computations as $M = 0.5, Sc = 5, Nc = 2, Nbt = 2, Pr = 1, Le = 5, \varepsilon = 0.2, \lambda = 0.5, \beta_1 = 1, Fr = 1, \zeta = 0.1, N = 0.6, G = 2.$

Results and Discussion:

The findings of this study are presented through a series of graphs, each illustrating a distinct aspect of two-dimensional magnetohydrodynamic flow of Casson fluids through a porous medium, incorporating the Darcy-Forchheimer model, over a stretching sheet. The graphical results focus on sensitivity analysis, examining the impact of key parameters – magnetic parameter (M), convection parameter (G), buoyancy ratio parameter (N), unsteadiness parameter (ζ), velocity ratio parameter (ϵ), and Casson parameter (β_1) – on thermophysical flow. The visual representation of results enables a thorough understanding of the phenomena and facilitates the drawing of meaningful conclusions.

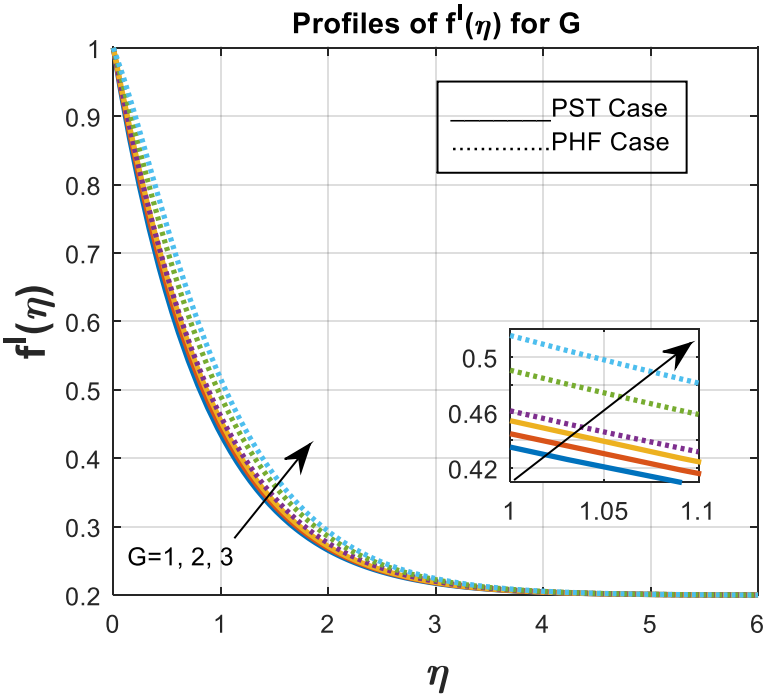

Figure 2: Impact of G (Thermal convection parameter) on Velocity Profile

Figure 2 illustrates the increasing in profile with increasing in G due to **Non-linear convection parameter**, driven by enhanced buoyancy-dominated fluid dynamics. When the thermal convection parameter increases, buoyancy forces that arise from temperature differences between the fluid and its surroundings become more significant. Stronger buoyancy forces drive more vigorous convective currents, with hot fluid rising and cold fluid sinking. This leads to more vigorous convection currents.

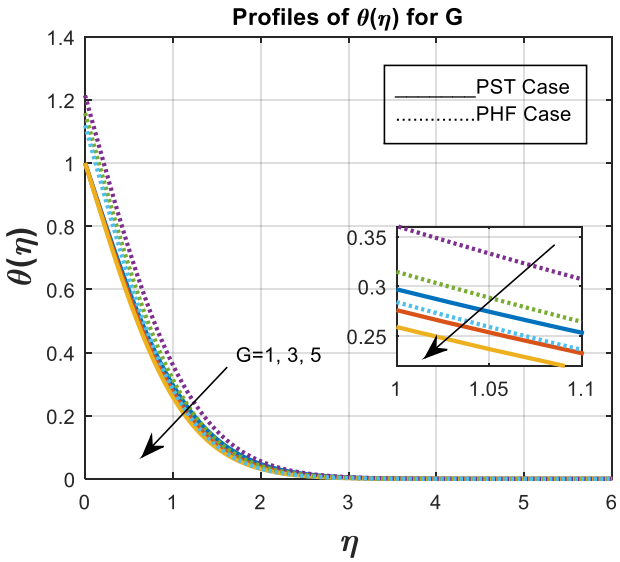

Figure 3: Impact of G (Thermal convection parameter) on Temperature Profile

Figure 3 illustrates the influence of G on the boundary layer and temperature profile. As G increases, θ(η) decreases, indicating a contraction of the boundary layer thickness due to enhanced temperature gradients. Concurrently, the fluid's temperature profile decreases, demonstrating the thermodynamic coupling between G and thermal transport.

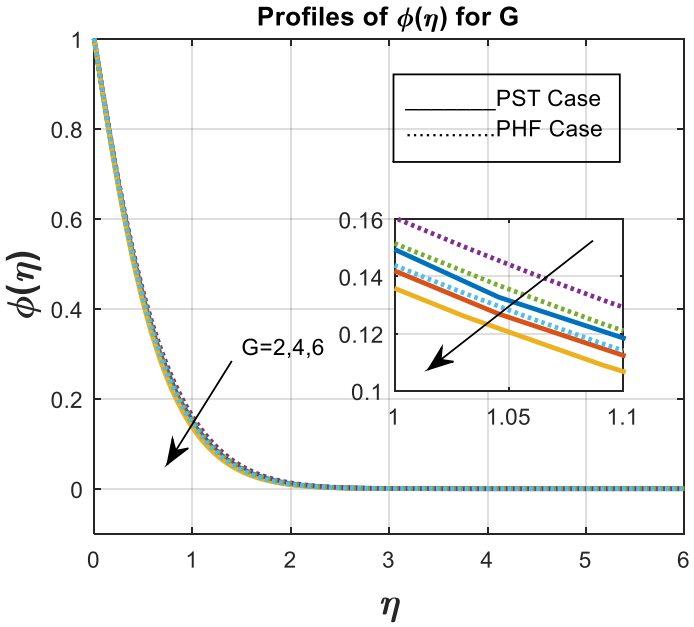

Figure 4: Impact of G (Thermal Convection parameter) on Concentration Profile

Figure 4 illustrates the impact of the thermal convection parameter on the concentration profile, highlighting its reduction due to a larger reaction rate parameter. As the thermal convection parameter increases, enhanced buoyancy forces drive more intense fluid motion, facilitating rapid mixing of species and a more uniform concentration distribution throughout the fluid. Consequently, the concentration gradient becomes less pronounced, departing from the characteristics of a purely diffusive system.

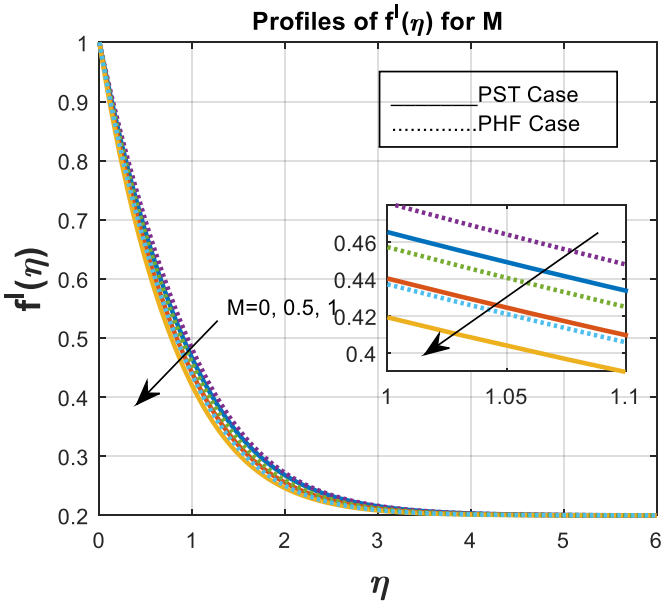

Figure 5: Impact of M (Magnetic Parameter) on Velocity Profile

Figure 5 depicts the decrease in velocity profile f'(η) with escalating magnetic field strength M. The applied magnetic field generates a Lorentz force that counteracts fluid motion, inducing magnetic damping that resists fluid flow. As the magnetic parameter (Hartmann number) increases, the conducting fluid interacts with the magnetic field, producing a resistive Lorentz force that opposes flow. Consequently, the fluid's velocity diminishes, particularly in the direction of the applied magnetic field, resulting in a more sluggish flow.

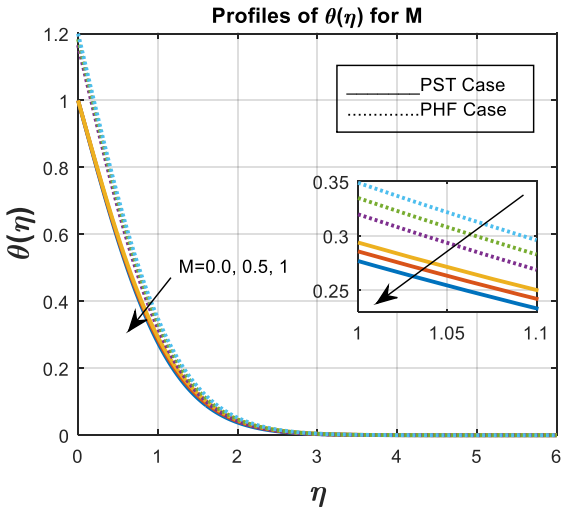

Figure 6: Impact of M (Magnetic Parameter) on Temperature Profile

Figure 6 demonstrates that the magnetic field's influence, characterized by increasing M, leads to an increase in θ(η), implying a rise in surface temperature due to magnetic drag. as the magnetic parameter increases, the temperature profile shifts from one dominated by convection (with steep gradients) to one controlled by diffusion (with more uniform temperature distribution), particularly in the bulk of the fluid. However, near the boundary or heat source, the temperature gradient remains sharp due to the relatively more efficient heat transfer within the Hartmann layer.

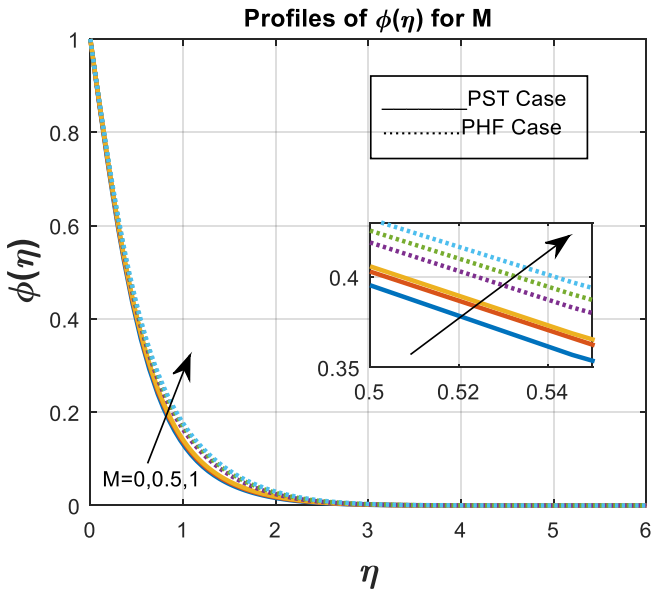

Figure 7: Impact of M (Magnetic Parameter) on Concentration Profile

Figure 7 illustrates the positive correlation between magnetic field strength (M) and concentration profile, indicating increased saturation in porous media. as the magnetic parameter increases, the concentration profile shifts from one dominated by convection (with sharp gradients) to one dominated by diffusion (with smoother, more gradual concentration gradients). The boundary layers may still have sharper gradients, but the bulk of the fluid will have a more uniform concentration due to the suppression of convective mixing.

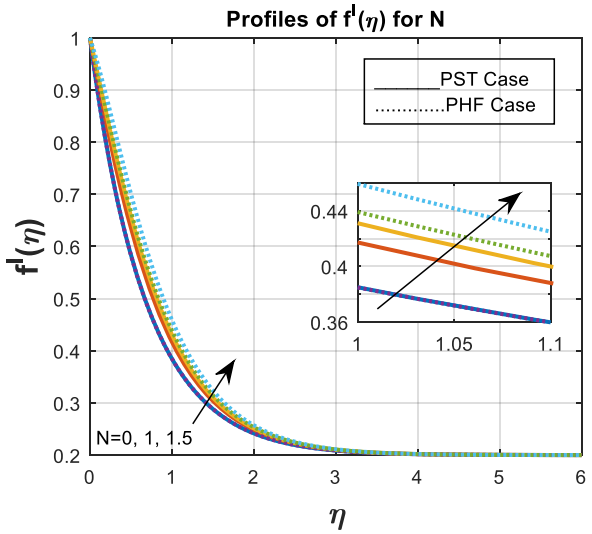

Figure 8: Impact of N (Buoyancy ratio parameter) on Velocity Profile

As shown in Figure 8, increased buoyancy forces (N) enhance fluid velocity. This is because buoyant forces are directly correlated with fluid density, which in turn is inversely correlated with fluid temperature. The Buoyancy Ratio Parameter determines the relative importance of thermal and compositional buoyancy forces in a fluid, significantly affecting the velocity profile. A high N leads

to vertical, thermal-dominant convection, while a low N results in lateral, solutal-dominant convection. The velocity profile transitions between these regimes based on the value of N.

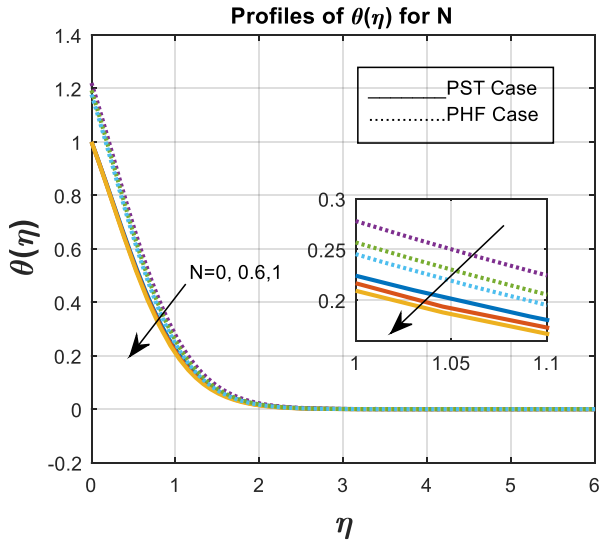

Figure 9: Impact of *N* (Buoyancy ratio parameter) on Temperature Profile

Figure 9 shows where shooting values of N show a noticeable fall in $\theta(\eta)$. Convection and temperature distribution are improved by an increase in fluid velocity, which is brought on by an increase in buoyant forces. $\theta(\eta)$ declines as a result. the Buoyancy Ratio Parameter N strongly influences the temperature profile. As N increases, thermal buoyancy dominates, leading to steeper temperature gradients and stronger thermal stratification. As N decreases, compositional buoyancy becomes more important, resulting in a more uniform temperature profile dominated by diffusion.

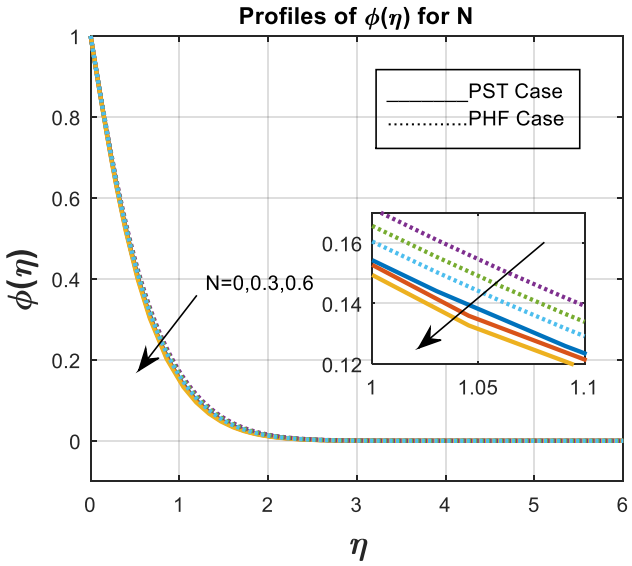

Figure 10: Impact of N (Buoyancy ratio Parameter) on Concentration Profile

The concentration profile drops for high N values, as observed in Figure 10. The concentration distribution is improved by increased buoyancy forces, which lowers the concentration profiles. the Buoyancy Ratio Parameter N directly impacts the concentration profile by altering the relative

importance of thermal and solutal buoyancy in the fluid's convection. A higher N (thermal-dominant) leads to a more uniform concentration profile, while a lower N (compositional-dominant) results in stronger concentration stratification.

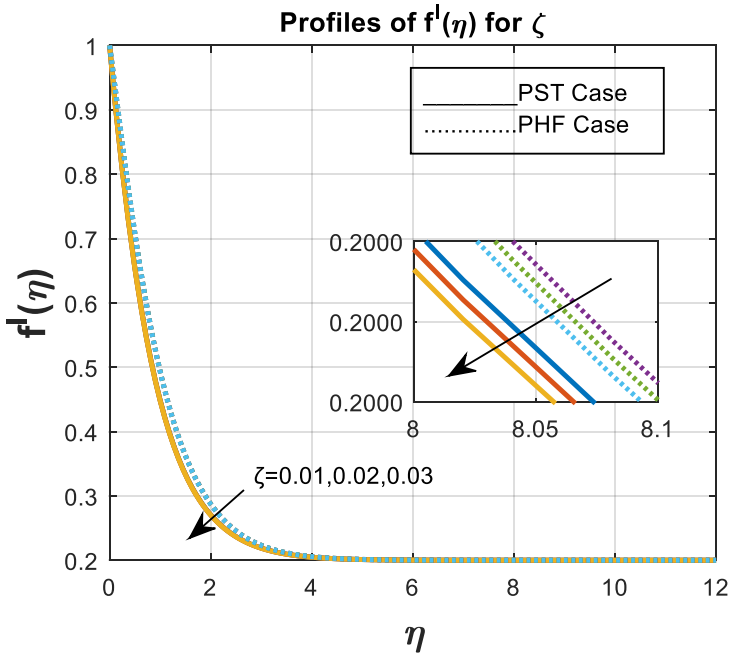

Figure 11: Impact of ζ (Unsteadiness parameter) on Velocity Profile

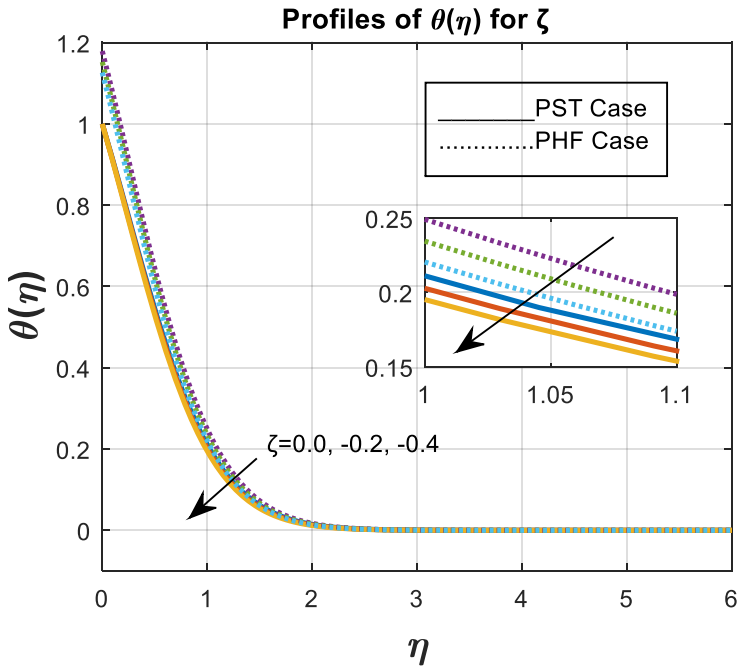

Figure 12: Impact of ζ (Unsteadiness parameter) on Temperature Profile

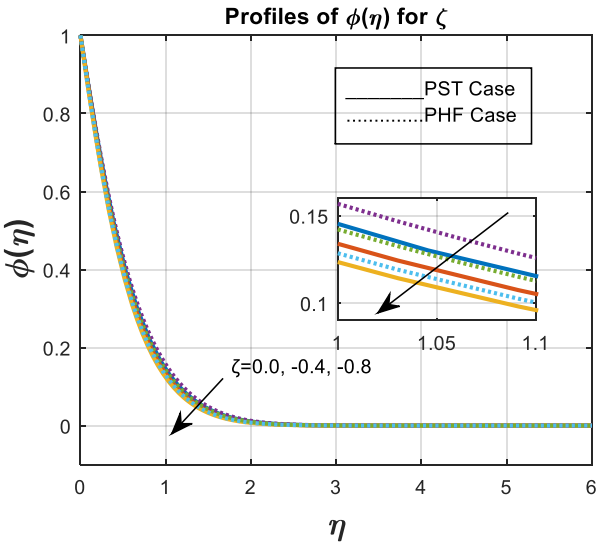

Figure 13: Impact of ζ (Unsteadiness parameter) on Concentration Profile

The fluid velocity increases with decreasing temperature. For rising rates of unsteadiness, $f'(\eta)$ exhibits a rather complex behaviour in Figure 11. Whereas $\zeta > 0$ denotes unsteadiness, $\zeta = 0$ represents the steady condition. The momentum thickness of the boundary layer near to stretching surface first appears to diminish as $f'(\eta)$ increases with ζ . As the rate of unsteadiness increases and the fluid motion becomes more intense, the fluid velocity and the boundary layer's thickness begin to grow.

Figures 12 and 13 illustrate the impact of the unsteadiness parameter on temperature and concentration profiles. Increasing the unsteadiness parameter leads to a decrease in both temperature and concentration profiles. This, in turn, reduces the thermal boundary layer thickness. However, beyond a certain distance from the surface, the temperature distribution expands with rising unsteadiness parameter values (ζ). This phenomenon is attributed to a decline in heat transfer rate near the surface, resulting in lower temperatures. A higher unsteadiness parameter enhances nanofluid molecule mobility, whereas lower unsteadiness leads to reduced agglomeration of fluid molecules. Consequently, diminished agglomeration results in less concentration dispersion.

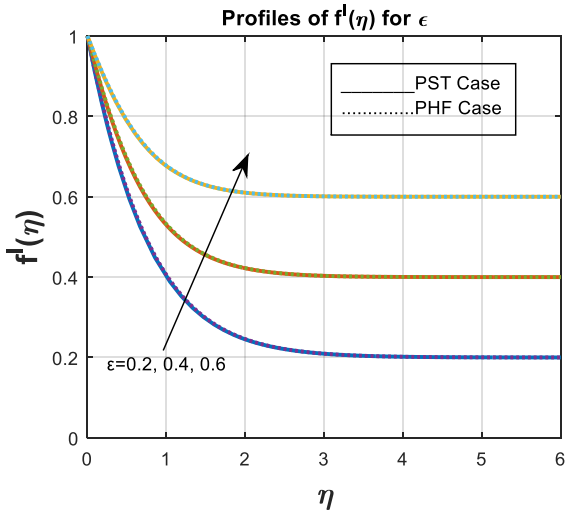

Figure 14: Impact of ε (Velocity ratio Parameter) on Velocity Profile

Figure 14 explores the impact of velocity ratio parameter on velocity profile, the greater external velocity causes a faster local heat transfer, which lowers the fluid's temperature. The **Velocity Ratio Parameter ε** significantly affects the **velocity profile** by determining the relative contributions of thermal and compositional buoyancy to the flow. A high ε (thermal-dominant) leads to a **vertical, temperature-driven flow**, while a low ε (compositional-dominant) leads to **horizontal flow**, influenced by concentration gradients.

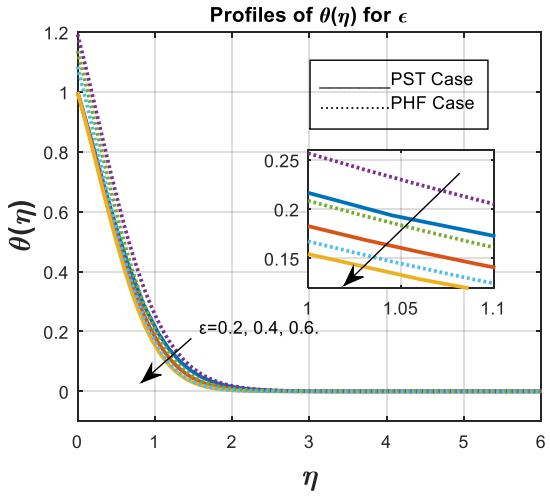

Figure 15: Impact of ε (Velocity ratio Parameter) on Temperature Profile

Figure 15 illustrates how θ(η) decreases significantly as ε rises, increase in a Velocity Ratio Parameter cause the increase in local heat transfer and reduced fluid temperature. compares the effects of different components of velocity in a fluid flow, typically in systems where both thermal and compositional buoyancy forces are present. The parameter primarily governs how the velocities driven by temperature differences (thermal buoyancy) and concentration differences (compositional buoyancy) interact and influence the flow behavior. When considering the effect of the Velocity Ratio Parameter on the temperature profile, it's essential to understand that the temperature profile is influenced by the velocity field, which in turn is governed by the relative dominance of thermal and compositional buoyancy forces.

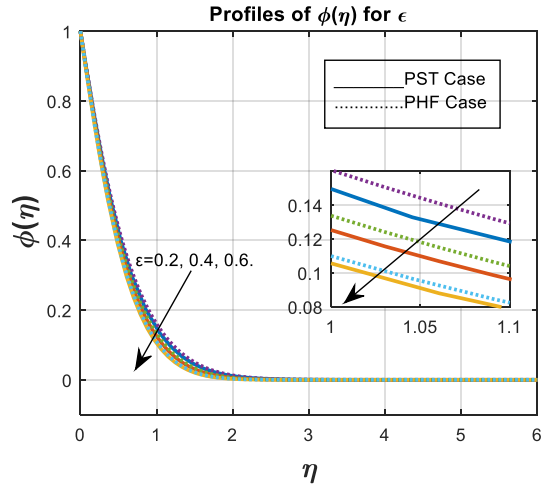

Figure 16: Impact of ε (Velocity ratio Parameter) on Concentration Profile

Figure 16 explores the impacts of the Velocity Ratio Parameter on the Concentration profile. Increase in Casson fluid parameter decrease in the Concentration profile. An increase in heat source retards the concentration profile, while a sink enhances it.

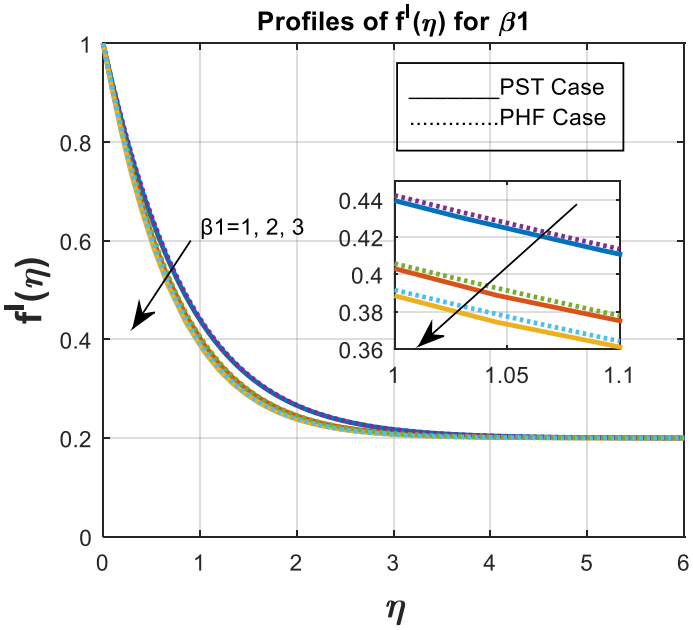

Figure 17: Impact of β_1(Casson fluid parameter) on Velocity Profile

Figure 17 explores the impacts of the Casson fluid parameter on the velocity profile. Increase in Casson fluid parameter decrease in the velocity profile. The Casson fluid parameter influences the velocity profile by modifying the fluid's resistance to flow. A higher Casson parameter (higher yield stress) leads to steeper velocity gradients near the wall and delays the flow in the core, whereas a lower Casson parameter (lower yield stress) allows for quicker flow initiation and a more uniform velocity profile, resembling the behavior of a Newtonian fluid.

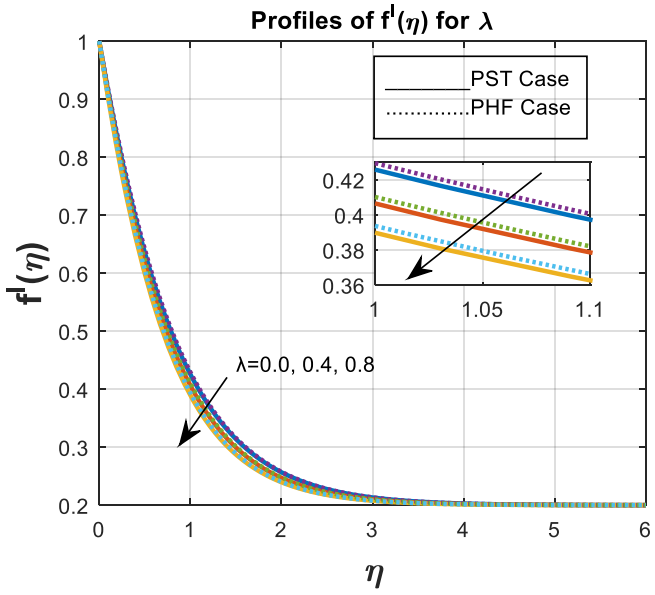

Figure 18: Impact of λ (Permeability parameter) on Velocity Profile

Figure 18 illustrates a evident falls in $f'(\eta)$, when λ increases. Increasing λ leads to increased velocity. λ also affects boundary layer thickness, with higher λ values resulting in thinner boundary layers. λ influences flow resistance, with higher λ values reducing resistance. Due to change in λ, velocity profile shape changes from parabolic (low λ) to more uniform (high λ).

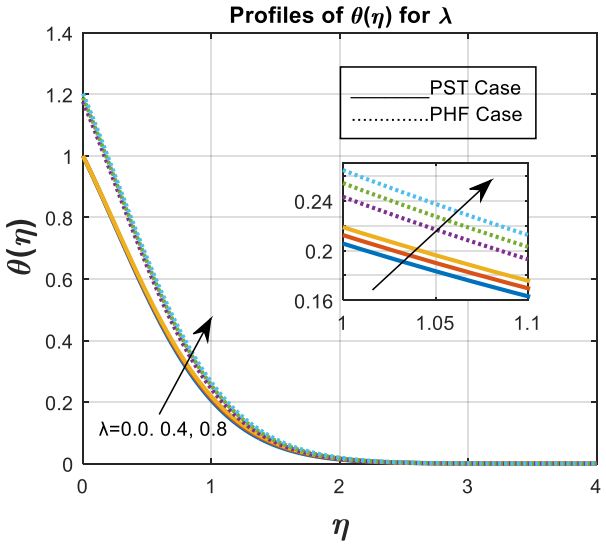

Figure 19: Impact of λ (Permeability Parameter) on Temperature Profile

Figure 19 demonstrates the impact of porous media on thermal boundary layer thickness and temperature profile θ(η), revealing increased flow resistance. Notably, θ(η) increases with rising λ values. The permeability parameter significantly influences the temperature profile in porous media. Higher permeability facilitates enhanced fluid flow, resulting in improved convective heat transfer and a more uniform temperature distribution. Conversely, lower permeability hinders fluid flow, leading to larger temperature gradients, reduced heat transport efficiency, and a dominance of conduction in the heat transfer process.

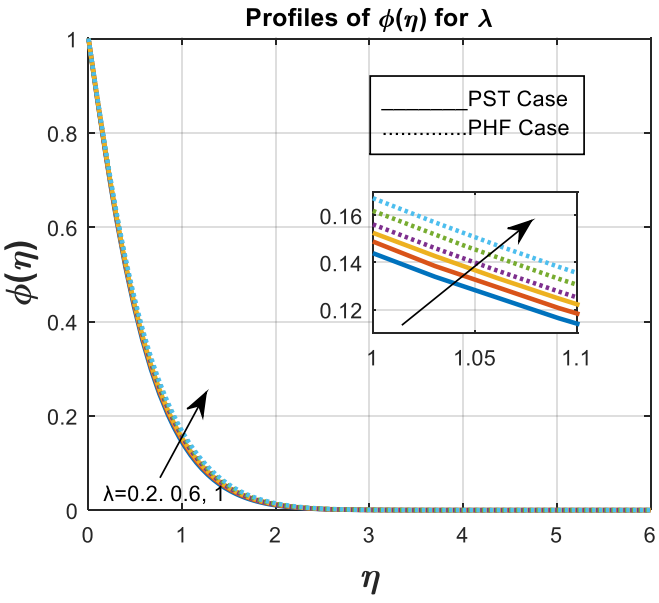

Figure 20: Impact of λ (Permeability Parameter) on Concentration Profile

Figure 20 demonstrates the impact of Permeability parameter λ on concentration profiles, revealing an increase in φ(η) with rising λ values. The permeability parameter strongly influences the concentration profile in porous media. High permeability leads to faster fluid flow, which enhances convective transport and results in a more uniform concentration profile. In contrast, low permeability leads to slower flow, causing diffusion to dominate, which results in larger concentration gradients and a more stratified concentration profile.

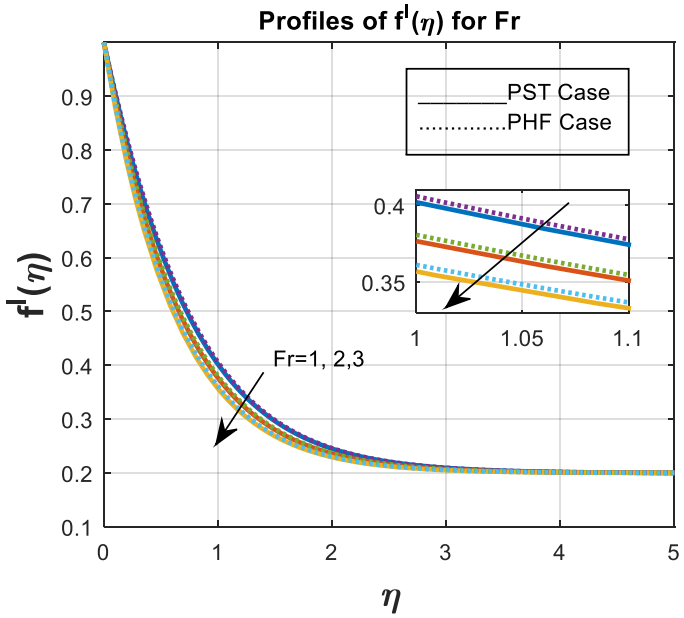

Figure 21: Impact of *Fr* (Forchheimer number) on Velocity Profile

The velocity profile is shown in Figure 21 to be decreasing as we increase Fr. The decrease in $f'(\eta)$ with rising Fr is due to the inverse relationship between $f'(\eta)$ and the permeability of porous media, which provides resistance to fluids and therefore slows their motion. The thickness of the boundary layers also shrunk.

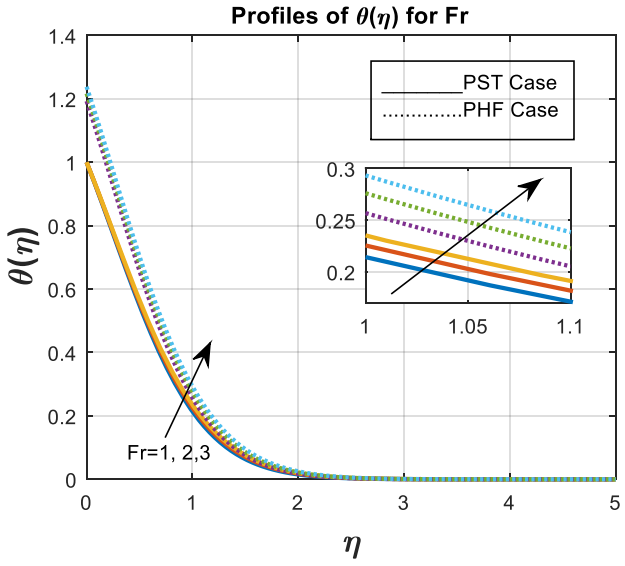

Figure 22: Impact of Fr (Forchheimer number) on Temperature Profile

Figure 22 illustrates a positive association between the temperature profile θ(η) and the Forchheimer number Fr, indicating a rise in θ(η) as Fr increases. The Forchheimer number significantly influences the temperature profile in porous media. In the case of low Forchheimer numbers (laminar flow), the temperature profile is more gradual with larger temperature gradients. As the Forchheimer number increases, the flow transitions to turbulent conditions, resulting in a more uniform temperature distribution with smaller temperature gradients due to enhanced convective heat transfer.

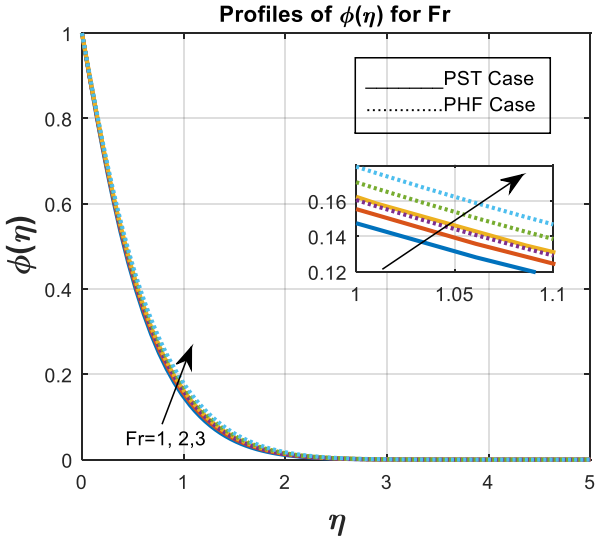

Figure 23: Impact of Fr (Forchheimer number) on Concentration Profile

Figure 23 demonstrates that the volume fraction profile increases monotonically with Forchheimer number (Fr), indicating nanoparticle migration away from the surface. The concentration profile in porous media is strongly dependent on the Forchheimer number. For low Forchheimer numbers, where the flow is laminar, the concentration profile is characterized by larger concentration gradients and thicker boundary layers due to slower solute transport. As the Forchheimer number increases and the flow transitions to turbulent or non-Darcy flow, the concentration profile becomes more uniform, with smaller concentration gradients and thinner boundary layers due to enhanced convective mixing.

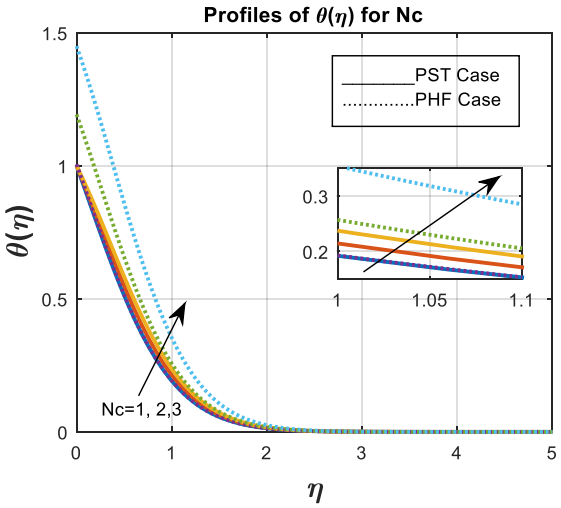

Figure 24: Impact of *Nc* on Temperature Profile

Figure 24 illustrates the positive correlation between θ(η) and Nc, highlighting the significant role of nanoparticle concentration in heat transfer enhancement. Variations in the concentration parameter can substantially alter the temperature profile of fluids. The interaction between solute concentration and fluid dynamics, along with its impact on heat transfer mechanisms (such as convection, diffusion, and reaction heat), can lead to changes in the uniformity, steepness, and boundary layer characteristics of the temperature profile. Depending on the context, these effects can either enhance or reduce the temperature gradients and influence heat distribution within the system.

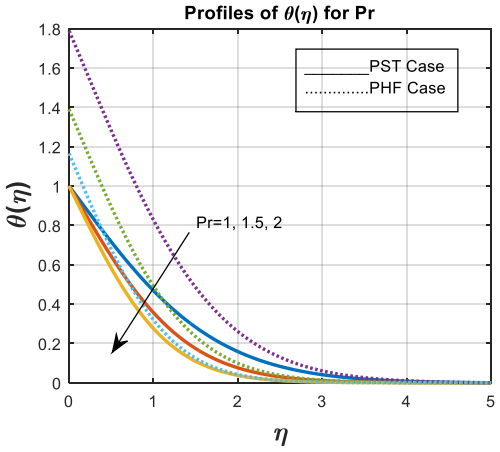

Figure 25: Impact of *Pr* on Temperature Profile

Figure 25 demonstrates how quickly heat diffuses when Pr > 1. This is because a lower thermal diffusivity, which is indicated by a greater Prandtl number, leads to a drop in the thermal boundary layer. The Prandtl number plays a crucial role in determining the temperature profile in fluid flow systems A low Prandtl number results in rapid heat diffusion, a reduced thermal boundary layer, and a more uniform temperature profile. High Prandtl numbers lead to a thicker thermal boundary layer, slower heat diffusion, and steeper temperature gradients near heat sources. For Pr ≈ 1, the fluid will exhibit a moderate temperature profile with a balance between the momentum and thermal diffusion rates. Understanding the Prandtl number is important for predicting how heat will distribute in a system, especially in engineering applications like heat exchangers, cooling systems, and fluid flow over surfaces.

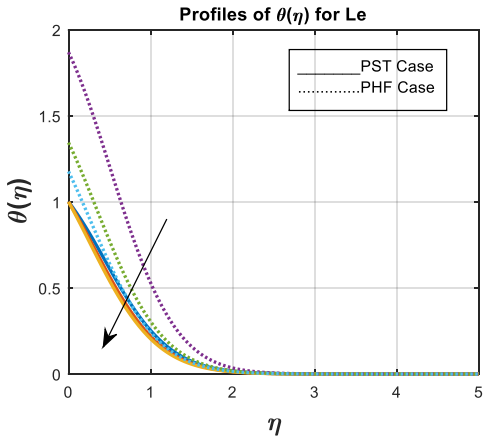

Figure 26: Impact of *Le* (Lewis number) on Temperature Profile

Figure 26 illustrates the inverse relationship between θ(η) and Lewis number (Le), demonstrating that temperature profile decreases as Le increases. and that a greater thermal diffusivity is related to a greater Lewis number (Le).

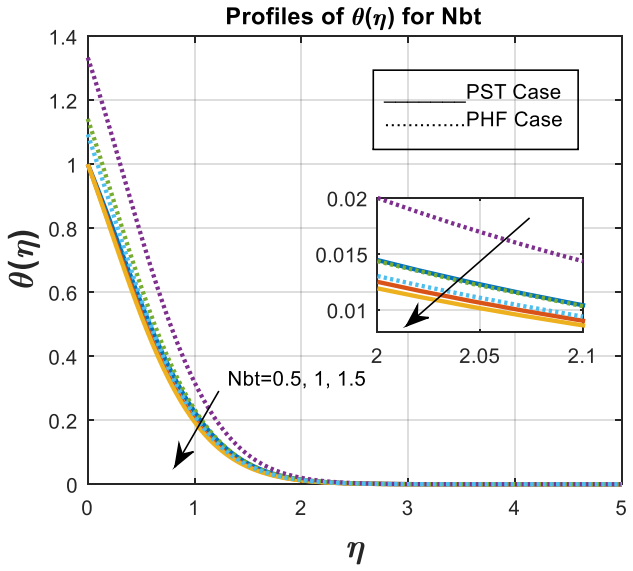

Figure 27: Impact of N_{bt} ((Diffusivity Parameter) on Temperature Profile

Figure 27 illustrates the decrease in temperature profile θ(η) as nanoparticle Brownian motion (N_{bt}) increases, The temperature profile typically follows this trend because of the correlation between the Brownian diffusivity and the diffusion coefficient of thermophoretic in the diffusivity ratio.

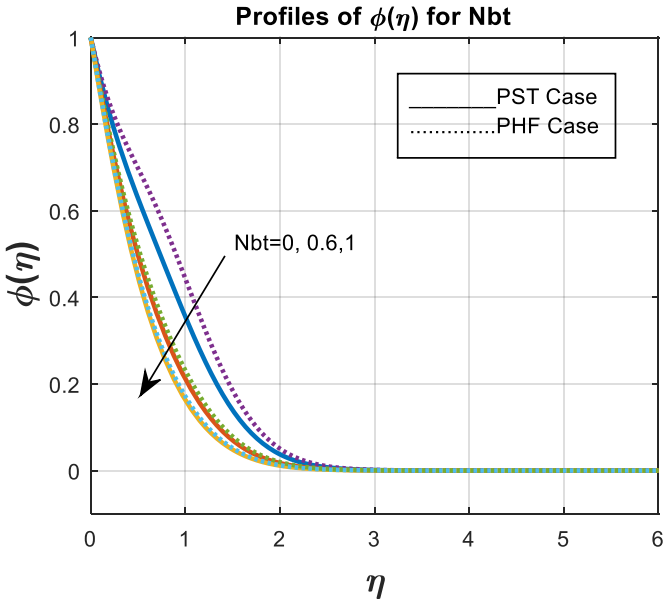

Figure 28: Impact of N_{bt} (Diffusivity Parameter) on Concentration Profile

Figure 28 demonstrates that growing Nbt values cause nanofluid particles to become more energetic, spreading out and reducing φ(η). The increasing amount of Nbt causes the nanofluid particles to move about a lot, which causes them to spread out and collide more frequently.

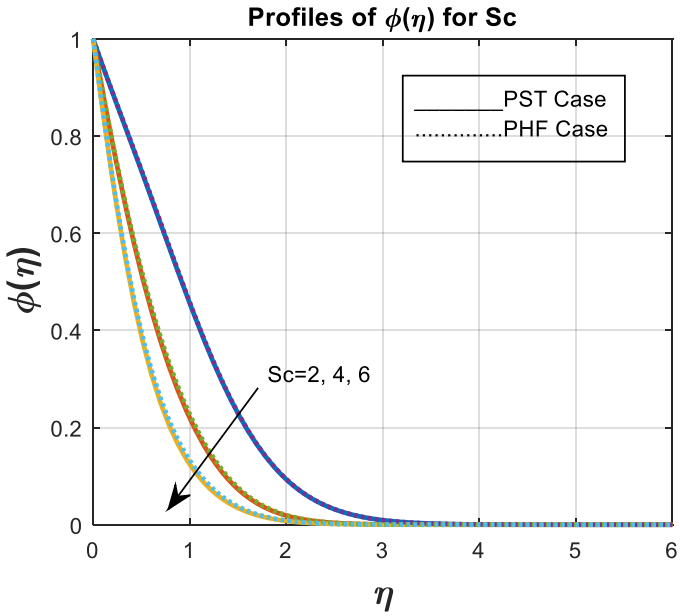

Figure 29: Impact of Sc (Schmidt number) on Concentration Profile

Figure 29 reveals that the Schmidt number significantly influences momentum and concentration boundary layers, with higher values suppressing Brownian diffusivity. Logically, Brownian diffusivity and Schmidt number exhibit an inverse relationship. A lower φ(η) results from a weaker Brownian diffusivity caused by a larger Schmidt number.

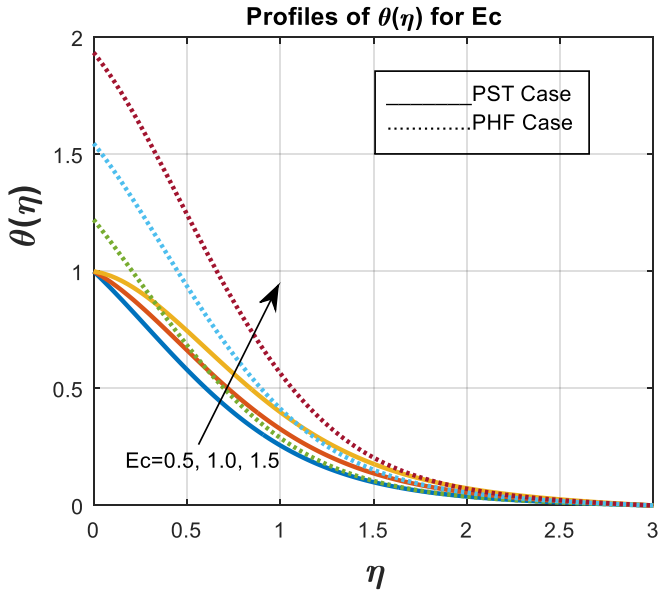

Figure 30: Impact of Ec (Eckert number) on Temperature Profile

Figure 30 demonstrates that a rise in the Eckert number corresponds to an increase in fluid temperature. The Eckert number serves as a crucial indicator of the significance of self-heating effects caused by dissipation, helping to determine whether these effects can be neglected. At high flow velocities, the temperature profile is affected by both temperature gradients and the effects of dissipation.

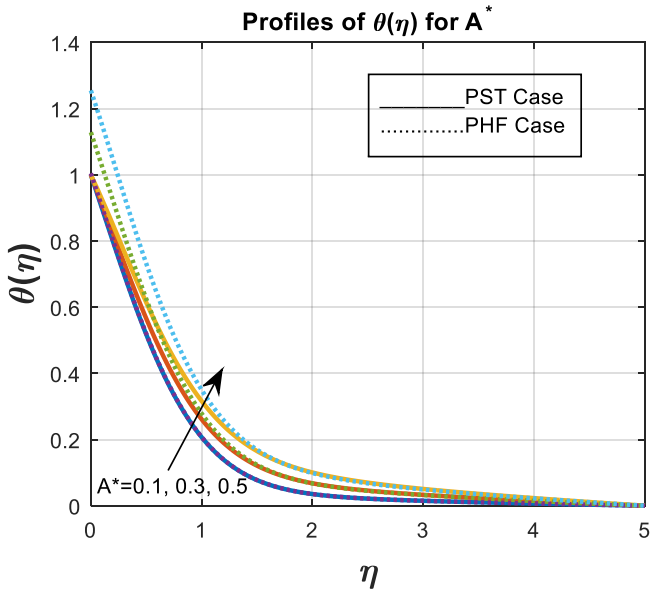

Figure 31: Impact of A^* on Temperature Profile

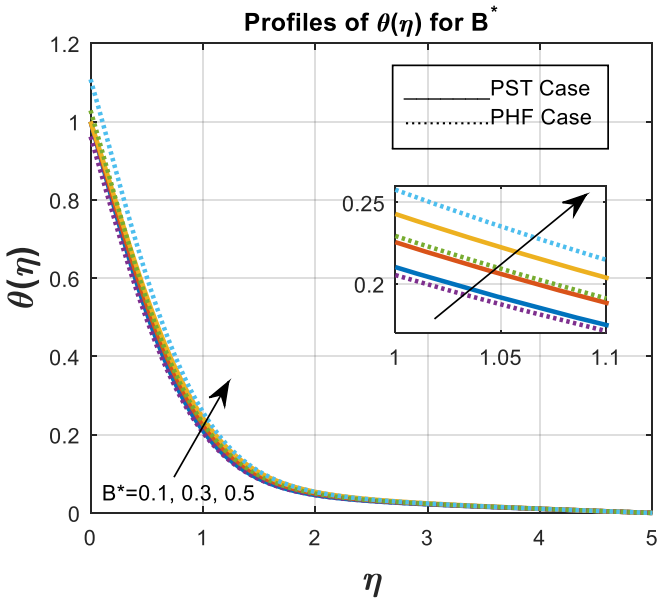

Figure 32: Impact of B^* on Temperature Profile

Figures 31 and 32 illustrate the effect of heat source/sink parameters A∗ and B∗ on temperature distribution θ(η). Notably, increasing A∗ and B∗ values yield a significant rise in fluid temperature, indicating enhanced heat generation within the flow. The temperature distribution is strongly correlated with the magnitude of A∗ and B∗.

Conclusion:

A comprehensive analysis of a two-dimensional, unsteady, incompressible MHD Casson fluid was conducted, focusing on its interactions with nanoparticles and non-uniform heat source/sink in the presence of chemical reactions. Assuming mass and heat transport across a stretching sheet, this study quantitatively examined the influence of various thermophysical parameters on velocity,

concentration, and temperature distributions. The key results of this investigation are summarized below.

- The magnetic field induces a resistive force, resulting in a reduction of fluid velocity, resulting in a more pronounced boundary layer near the wall.
- Due to non-Newtonian nature of Casson fluids, the yield stress of the Casson fluid affects the overall flow resistance and modifies the velocity and temperature profiles compared to Newtonian fluids. Higher yield stress generally results in reduced velocity fields and altered thermal profiles.
- Forchheimer term becomes increasingly significant at higher velocities, leading to a more complex flow pattern and a more pronounced impact on heat transfer.
- Heat sources affect the temperature distribution within the fluid. The temperature gradient and the resulting heat transfer rates are strongly influenced by the interaction between the heat sources and the convective flow.
- The concurrent influence of the magnetic field, Casson fluid properties, porous medium resistance, and heat sources lead to complex interactions that dictate the thermal and flow behavior.
- As Joule heating (J) increases, both momentum and temperature curves exhibit a significant upward trend.
- The momentum and temperature curves exhibit a significant increase with the enhancement of variable heat source/sink parameters, specifically A* and B*.

References

1. Crane, Lawrence J. "Flow past a stretching plate." *Zeitschrift für angewandte Mathematik und Physik ZAMP* 21 (1970): 645-647.
2. Sakiadis, Byron C. "Boundary-layer behavior on continuous solid surfaces: I. Boundary-layer equations for two-dimensional and axisymmetric flow." *AIChE Journal* 7.1 (1961): 26-28.
3. Farooq, Umer, et al. "Impact of non-similar modeling on Darcy-Forchheimer-Brinkman model for forced convection of Casson nano-fluid in non-Darcy porous media." *International Communications in Heat and Mass Transfer* 125 (2021): 105312.
4. Shoaib, Muhammad, et al. "MHD casson nanofluid in darcy-forchheimer porous medium in the presence of heat source and arrhenious activation energy: applications of neural networks." *International Journal of Modelling and Simulation* 43.4 (2023): 438-461.
5. Shoaib, Muhammad, et al. "Impact of thermal energy on MHD Casson fluid through a Forchheimer porous medium with inclined non-linear surface: A soft computing approach." *Alexandria Engineering Journal* 61.12 (2022): 12211-12228.
6. Farooq, Umer, et al. "Modeling and non-similar analysis for Darcy-Forchheimer-Brinkman model of Casson fluid in a porous media." *International Communications in Heat and Mass Transfer* 119 (2020): 104955.
7. Seth, Gauri Shanker, et al. "Double diffusive MHD Casson fluid flow in a non-Darcy porous medium with Newtonian heating and thermo-diffusion effects." *International Journal of Heat & Technology* 36.4 (2018).
8. Durairaj, Mythili, Sivaraj Ramachandran, and Rashidi Mohammad Mehdi. "Heat generating/absorbing and chemically reacting Casson fluid flow over a vertical cone and flat plate

saturated with non-Darcy porous medium." *International Journal of Numerical Methods for Heat & Fluid Flow* 27.1 (2017): 156-173.

9. Jat, Kavita, et al. "Significance of Darcy–forchheimer Casson fluid flow past a non-permeable curved stretching sheet with the impacts of heat and mass transfer." *Case Studies in Thermal Engineering* 61 (2024): 104907.
10. Waheed, Shimaa E., Galal M. Moatimid, and Abeer S. Elfeshawey. "Unsteady magnetohydrodynamic squeezing Darcy-Forchheimer flow of Fe3O4 Casson nanofluid: Impact of heat source/sink and thermal radiation." *Partial Differential Equations in Applied Mathematics* 10 (2024): 100666.
11. Sharma, Kushal, et al. "Dynamics of MHD Casson fluid in non-Darcy porous medium: The impact of thermal radiation, Dufour–Soret, and chemical reaction." *Modern Physics Letters B* 38.16 (2024): 2341007.
12. Ragupathi, P., et al. "Application of Arrhenius kinetics on MHD radiative Von Kármán Casson nanofluid flow occurring in a Darcy-Forchheimer porous medium in the presence of an adjustable heat source." *Physica Scripta* 96.12 (2021): 125228.
13. Li, Shuguang, et al. "Effects of activation energy and chemical reaction on unsteady MHD dissipative Darcy–Forchheimer squeezed flow of Casson fluid over horizontal channel." *Scientific reports* 13.1 (2023): 2666.
14. Faisal, Muhammad, Iftikhar Ahmad, and Tariq Javed. "Numerical assessments of prescribed heat sources on unsteady 3D flow of Williamson nanoliquid through porous media." *Special Topics & Reviews in Porous Media: An International Journal* 12.2 (2021).
15. Tufail, Muhammad Nazim, Musharafa Saleem, and Qasim Ali Chaudhry. "Chemically reacting mixed convective Casson fluid flow in the presence of MHD and porous medium through group theoretical analysis." *Heat Transfer* 49.8 (2020): 4657-4677.
16. Mohamed, R. A., et al. "MHD Casson nanofluid flow over a stretching surface embedded in a porous medium: effects of thermal radiation and slip conditions." *Latin Am. Appl. Res* 51 (2021): 229-239.
17. Ramesh, Gosikere Kenchappa. "Darcy-Forchheimer flow of Casson nanofluid with heat source/sink: a three-dimensional study." *Heat and mass transfer-advances in modelling and experimental study for industrial applications, London: Intech Open* (2018): 43-62.
18. Abbas, Amir, Mdi Begum Jeelani, and Nadiyah Hussain Alharthi. "Darcy–Forchheimer relation influence on MHD dissipative third-grade fluid flow and heat transfer in porous medium with joule heating effects: A numerical approach." *Processes* 10.5 (2022): 906.
19. Kala, Bhim Sen. "The numerical investigation of Effects of Darcy and Forchheimer parameters on Magnetohydrodynamic Casson fluid flow through non-Darcy porous media." *International Journal of Mathematics Trends and Technology-IJMTT* 40 (2016).
20. Eid, Mohamed R. "Thermal characteristics of 3D nanofluid flow over a convectively heated Riga surface in a Darcy–Forchheimer porous material with linear thermal radiation: an optimal analysis." *Arabian Journal for Science and Engineering* 45.11 (2020): 9803-9814.
21. Shampine, Lawrence F., Jacek Kierzenka, and Mark W. Reichelt. "Solving boundary value problems for ordinary differential equations in MATLAB with bvp4c." *Tutorial notes* 2000 (2000): 1-27.

22. Devi, Rekha, and Shilpa Sood. "Convective MHD flow of Casson fluid through porous medium using the Darcy-Forchheimer model under the impact of prescribed heat sources." *ZAMM-Journal of Applied Mathematics and Mechanics/Zeitschrift für Angewandte Mathematik und Mechanik* (2024): e202300344.
23. Mustafa, M., et al. "Unsteady boundary layer flow of a Casson fluid due to an impulsively started moving flat plate." *Heat Transfer—Asian Research* 40.6 (2011): 563-576.
24. Eldabe, Nabil TM, G. Saddeck, and A. F. El-Sayed. "Heat transfer of MHD non-Newtonian Casson fluid flow between two rotating cylinders." *Mechanics and Mechanical Engineering* 5.2 (2001): 237-251.
25. Ishak, Anuar, Roslinda Nazar, and I. Pop. "Mixed convection on the stagnation point flow toward a vertical, continuously stretching sheet." (2007): 1087-1090.
26. Bejawada, Shankar Goud, et al. "Radiation effect on MHD Casson fluid flow over an inclined non-linear surface with chemical reaction in a Forchheimer porous medium." *Alexandria Engineering Journal* 61.10 (2022): 8207-8220.
27. Thakur, Archie, and Shilpa Sood. "Effect of prescribed heat sources on convective unsteady MHD flow of Williamson nanofluid through porous media: Darcy–Forchheimer Model." *International Journal of Applied and Computational Mathematics* 8.2 (2022): 74.
28. Majeed, A., A. Zeeshan, and R. Ellahi. "Unsteady ferromagnetic liquid flow and heat transfer analysis over a stretching sheet with the effect of dipole and prescribed heat flux." *Journal of Molecular liquids* 223 (2016): 528-533.